Draft version October 20, 2016
Preprint typeset using LaTeX style emulateapj v. 11/10/09

arXiv:1610.05978v1 [astro-ph.GA] 19 Oct 2016

NEAR-INFRARED SPECTROSCOPY OF NEARBY SEYFERT GALAXIES: IS THERE EVIDENCE FOR THE SHOCK EXCITATION IN NARROW-LINE REGIONS?

K. Terao[1], T. Nagao[2], T. Hashimoto[3], K. Yanagisawa[4], K. Matsuoka[5], Y. Toba[2,6], H. Ikeda[7], and Y. Taniguchi[8]

Draft version October 20, 2016

ABSTRACT

One of the unsettled, important problems in active galactic nuclei (AGNs) is the major ionization mechanism of gas clouds in their narrow-line regions (NLRs). In order to investigate this issue, we present our J-band spectroscopic observations for a sample of 26 nearby Seyfert galaxies. In our study, we use the flux ratio of the following two forbidden emission lines, [Fe II]1.257μm and [P II]1.188μm because it is known that this ratio is sensitive to the ionization mechanism. We obtain the [Fe II]/[P II] flux ratio or its lower limit for 19 objects. In addition to our data, we compile this flux ratio (or its lower limit) of 23 nearby Seyfert galaxies from the literature. Based on the collected data, we find that three Seyfert galaxies show very large lower limits of [Fe II]/[P II] flux ratios ($\gtrsim$10); NGC 2782, 5005, and Mrk 463. It is thus suggested that the contribution of the fast shock in the gas excitation is significantly large for them. However, more than half of Seyfert galaxies in our sample show moderate [Fe II]/[P II] flux ratios ($\sim$2), that is consistent to the pure photoionization by power-law ionizing continuum emission. We also find that the [Fe II]/[P II] flux ratio shows no clear correlation with the radio loudness, suggesting that the radio jet is not the primary origin of shocks in NLRs of Seyfert galaxies.

Subject headings: galaxies: active — galaxies: nuclei — galaxies: Seyfert — infrared: galaxies

1. INTRODUCTION

For these two decades, it has been observationally suggested that the evolution of galaxies is intimately related to the growth of supermassive black holes (SMBHs) in galactic nuclei based on various scaling relations between the mass of SMBHs ($M_{\rm BH}$) and properties of their host galaxies (e.g., Magorrian et al. 1998; Marconi & Hunt 2003; Di Matteo et al. 2005; see, for reviews, Kormendy & Richstone 1995; Kormendy & Ho 2013). It is also known that a significant fraction of galaxies shows the nuclear activity that is driven by the gas accretion onto a SMBH (Rees 1984; Ho et al. 1997b). Such active galactic nuclei (AGNs) emit huge radiative energy. In addition to the strong radiation, AGNs sometimes show strong outflows in various forms that are recognized as the radio jet (e.g., Wilson & Willis 1980; Gallimore et al. 2006), broad absorption-line (BAL) feature (e.g., Weymann et al. 1991; Gibson et al. 2009), ultra-fast outflow (UFO; e.g., Cappi 2006; Tombesi et al. 2010), and so on. The released radiative and mechanical energies are expected to give significant impacts on various properties of the inter-stellar medium (ISM) in host galaxies, that may lead to the termination of the star-forming activity. This "AGN feedback" possibly takes an important role in the galaxy-SMBH coevolution, and therefore extensive observational efforts have been made to understand the AGN feedback phenomena (see Fabian 2012 for a review).

For studying the AGN feedback, one interesting approach is focusing on the narrow-line region (NLR) in AGNs. This is because (1) the typical spatial scale of the NLR is $\sim 10^{1-4}$ pc, covering the spatial scale of host galaxies, and (2) the ionized gas clouds in the NLR radiate a variety of emission lines that enable us to diagnose physical and chemical properties of the ISM in NLRs. It is widely believed that the dominant ionization mechanism of ionized gas clouds in NLRs is the photoionization by ionizing photons from the AGN central engine (e.g., Binette et al. 1996; Komossa & Schulz 1997; Groves et al. 2004). However it has been sometimes claimed that the fast shocks may also contribute significantly to the ionization in NLRs of some AGNs (e.g., Knop et al. 1996; Bicknell et al. 1998; Wilson & Raymond 1999; Fu & Stockton 2007). The discrimination of ionization mechanisms of gas clouds in the NLR is important in terms of the AGN feedback, because it is closely related to the question either radiative or mechanical heating is important for the gas in NLRs. Unfortunately, emission-line diagnostics in the rest-frame optical and ultraviolet range are not powerful to discriminate the ionization mechanism of NLR gas clouds, since the photoionization by the power-law spectral energy distribution (SED) and the fast shock result in very similar emission-line flux ratios (e.g., Dopita & Sutherland 1995, 1996; Allen et al. 2008).

A powerful method to distinguish the ionization mechanism of NLR gas clouds was proposed by Oliva et al.

terao@cosmos.phys.sci.ehime-u.ac.jp
[1] Graduate School of Science and Engineering, Ehime University, Bunkyo-cho 2-5, Matsuyama, Ehime 790-8577, Japan
[2] Research Center for Space and Cosmic Evolution, Ehime University, Bunkyo-cho 2-5, Matsuyama, Ehime 790-8577, Japan
[3] National Tsing Hua University, No. 101, Section 2, Kuang-Fu Road, Hsinchu, 30013, Taiwan
[4] Okayama Astrophysical Observatory, National Astronomical Observatory of Japan, Honjo 3037-5, Kamogata-cho, Asaguchi, Okayama 719-0232, Japan
[5] Department of Astronomy, Kyoto University, Kitashirakawa-Oiwake-cho, Sakyo-ku, Kyoto 606-8502, Japan
[6] Institute of Astronomy and Astrophysics, Academia Sinica, PO Box 23-141, Taipei 10617, Taiwan
[7] National Astronomical Observatory of Japan, Osawa 2-21-1, Mitaka, Tokyo, 181-8588, Japan
[8] The Open University of Japan, Wakaba 2-11, Mihama-ku, Chiba 261-8586, Japan

(2001). They reported that the flux ratio of two forbidden emission lines seen in near-infrared J-band, [P II]1.188μm and [Fe II]1.257μm, is useful to distinguish the ionization mechanism. The reason is as follows. These two transitions have similar critical densities ($n_{\rm cr} = 5.3\times10^4$ cm^{-3} for [P II]1.188μm and $n_{\rm cr} = 3.5\times10^4$ cm^{-3} for [Fe II]1.257μm at 10,000 K; Koo et al. 2013), and the ionization potentials of the related ions are both below 13.6 eV that is the hydrogen ionization potential (7.9 eV for [Fe II] and 10.5 eV for [P II]). Therefore these two lines should arise at similar locations in NLRs; more specifically, they are both mainly from the partially-ionized gas (see, e.g., Mouri et al. 2000). Consequently their flux ratio should be almost proportional to the gas-phase abundance ratio of the phosphorus and iron. Here the iron is a well known refractory species, and thus most of iron is locked into dust grains usually. On the other hand, the depletion of phosphorus onto dust grains is only moderate (see, e.g., Cardelli et al. 1991). This means that the gas-phase elemental abundance ratio of the iron to the phosphorus in NLR gas clouds photoionized by the power-law ionizing radiation is significantly lower than the solar elemental abundance ratio due to the selective depletion of the iron. However dust grains are easily destroyed due to fast shocks, and thus the relative abundance of the gas-phase iron in shock-dominated NLRs should be much higher than that in photoionized gas clouds. Therefore, the flux ratio of [Fe II]/[P II] is expected to be much higher in shock-dominated clouds ($\gtrsim$ 20) than in photoionized clouds ($\sim$ 2). Observations of nearby AGNs show that the measured [Fe II]/[P II] flux ratio is actually in the range of $\sim$2–20 (Storchi-Bergmann et al. 2009; Riffel et al. 2010; Riffel & Storchi-Bergmann 2011; Schönell et al. 2014), and the flux ratio varies also with the location in the NLR (e.g., Storchi-Bergmann et al. 2009; Riffel et al. 2010, 2014, 2015; Hashimoto et al. 2011; Riffel & Storchi-Bergmann 2011; Schönell et al. 2014). Note that this flux ratio is totally free from the dust reddening thanks to the narrow wavelength separation between the two lines, which makes this flux ratio a powerful diagnostic tool for investigating the ionization mechanism of NLRs.

Though the [Fe II]/[P II] flux ratio is an interesting tool to explore the nature of the AGN feedback at the NLR scale, this emission-line flux ratio has not been measured in many objects so far ($\sim$ 20 objects; e.g., Oliva et al. 2001; Ramos Almeida et al. 2006, 2009; Riffel et al. 2006, 2013; Jackson & Beswick 2007; Krajnović et al. 2007; Hashimoto et al. 2011; Riffel & Storchi-Bergmann 2011; Schönell et al. 2014; Riffel et al. 2015). Therefore it is hard to carry out various statistical analyses on the [Fe II]/[P II] flux ratio currently. Also the small sample size does not allow us to investigate possible connections between the NLR ionization and AGN outflows such as the radio jet, BAL, and UFO, given the fact that the fraction of AGNs showing those outflow features is relatively low ($\sim$10% for radio jets, $\sim$10% for BALs, and $\sim$35% for UFOs; see, e.g., Tombesi et al. 2010).

In this paper, we present the result of our J-band spectroscopic observations of the central region in a number of nearby Seyfert galaxies aiming at investigating the [Fe II]/[P II] flux ratio and examining the ionization mechanism of gas clouds in the NLR. In Section 2, we describe the details of our observations and the data reduction procedure. In Section 3, we summarize the obtained results. We discuss the implications of our results in Section 4, and then we give the conclusion in Section 5.

2. OBSERVATIONS AND DATA REDUCTION

The targets were selected based on the optical [O III]λ5007 flux (given by Whittle 1992; Ho et al. 1997a; Risaliti et al. 1999) for focusing on objects with relatively strong NLR emission lines. Near-infrared longslit spectroscopic observations were carried out for 26 nearby Seyfert galaxies and associated standard stars (for correcting the telluric absorption features and the wavelength dependence of the sensitivity) from August 2010 to April 2011 with ISLE (Yanagisawa et al. 2006, 2008), a near-infrared imager and spectrograph for the Cassegrain focus of the 188 cm telescope at Okayama Astrophysical observatory (OAO). The detector (a HAWAII 1k $\times$ 1k array) provides a $4'.3 \times 4'.3$ field of view with $0''.25$ pixel^{-1} spatial sampling. The observations were performed in J-band (1.11$-$1.32μm) with using a $2''.0$-width longslit, and the typical nodding width was $\sim 30''$ ($\sim$120 pixels). The slit was oriented to PA=90° (E-W) for all targets. The unit exposure time was 120 sec, and the total on-source integration times for science targets was 18–288 min, depending on the target. The achieved spectral resolution is $\sim$ 1300, that is measured from the width of observed OH airglow emission lines. The typical seeing size was $\sim 1''.0 - 2''.0$, that is inferred from the spatial extension of standard stars on the 2 dimensional spectra. We summarize the redshifts, J-band magnitude, the AGN activity type, total exposure time, date of observations for each target, and also the corresponding standard star, in Table 1.

The data analysis was performed with using IRAF software (Tody 1986, 1993) by the standard manner; i.e., the flat fielding, background subtraction, stacking the individual spectra, spectral extraction from 2 dimensional spectra, wavelength calibration, correction for the atmospheric absorption and sensitivity function using the spectra of standard stars, and finally the conversion of the spectra from the observed frame to the rest frame. We adopted a $2''.0$ (8 pixels) aperture for the spectral extraction, by taking account of the seeing size during the observations. The magnitude and spectral type of standard stars were collected from the 2MASS (*Two Micron All Sky Survey*) All-Sky Catalog of Point Sources (Cutri et al. 2003) and the Hipparcos and Tycho catalogues (ESA 1997), respectively. During the process of the correction for the atmospheric absorption and sensitivity function, a blackbody spectrum with the temperature corresponding to the spectral type was assumed as the intrinsic spectrum. The fluxes, central wavelengths, and FWHMs (full width at half maximums) for the detected emission lines were measured with an IRAF command `splot`, assuming a single Gaussian for each emission line. For undetected emission lines, we calculate the 3σ flux upper limit based on the rms of the spectra around the expected wavelength assuming a velocity width of 500 km s^{-1} in FWHM, that is the typical value for detected emission lines in our observations.

TABLE 1
Observation log

Name	z[a]	m_J[b] (mag)	Type[c]	Exposure time (min)	Date	Standard star[d]	m_J[e] (mag)
NGC 1667	0.0152	9.92	Sy 2	114	2011 January 13	HIP 20507 (A2V)	5.09
NGC 2273	0.0061	9.45	Sy 2	94	2011 January 15, 16	HIP 30060 (A2V)	4.28
NGC 2782	0.0085	9.79	Sy 2	552	2011 January 13, 15	HIP 45590 (A1V)	5.76
					2011 March 24, 27		
NGC 3079	0.0037	8.44	Sy 2	68	2011 January 12	HIP 47006 (A2V)	4.63
NGC 3982	0.0037	9.77	Sy 1.9	18	2011 April 25	HIP 62402 (A9V)	5.45
NGC 4102	0.0028	8.76	LINER	110	2011 April 21, 28	HIP 62402 (A9V)	5.45
NGC 4169	0.0126	10.06	Sy 2	68	2011 January 12	HIP 60746 (A4V)	4.80
NGC 4192	−0.0005	7.82	LINER	48	2011 April 26	HIP 59819 (A3V)	5.17
NGC 4258	0.0015	6.38	Sy 2	48	2011 April 23	HIP 64906 (A0V)	5.15
NGC 4388	0.0084	8.98	Sy 2	36	2011 April 24	HIP 59819 (A3V)	5.17
NGC 4419	−0.0009	8.78	LINER[f]	60	2011 April 24	HIP 59819 (A3V)	5.17
NGC 4941	0.0037	9.09	Sy 2	48	2011 April 24	HIP 62983 (A2V)	5.87
NGC 5005	0.0032	7.46	LINER	100	2011 April 23	HIP 62641 (A3V)	5.40
NGC 5194	0.0015	6.40	Sy 2	168	2010 August 14−18	HIP 66234 (A5V)	4.53
NGC 5506	0.0062	9.71	Sy 2	212	2011 April 23, 28	HIP 68092 (A8V)	5.45
NGC 6500	0.0100	10.13	LINER	208	2010 August 16−18	HIP 91118 (A0V)	5.63
						HIP 87192 (A1V)	5.99
NGC 6951	0.0048	8.31	Sy 2	74	2010 August 12	HIP 102253 (A8V)	5.18
Mrk 3	0.0135	10.03	Sy 2	56	2011 January 12	HIP 29997 (A0V)	4.97
Mrk 6	0.0188	11.08	Sy 1.5	64	2011 January 13	HIP 29997 (A0V)	4.97
Mrk 34	0.0505	12.77	Sy 2	26	2011 April 26	HIP 52478 (A0V)	5.80
Mrk 463	0.0504	12.16	Sy 2	160	2011 April 24, 26, 28	HIP 68276 (A0V)	5.67
Mrk 477	0.0377	12.95	Sy 2	84	2010 August 10, 12	HIP 71573 (A1V)	5.76
Mrk 509	0.0344	11.58	Sy 1.5	166	2010 August 14, 15	HIP 102618 (A1V)	3.85
Mrk 766	0.0129	11.10	Sy 1	84	2011 April 26	HIP 60746 (A4V)	4.80
Mrk 1073	0.0233	11.26	Sy 2	288	2010 August 12, 14−18	HIP 15648 (A3V)	4.80
MCG +08-11-011	0.0205	10.49	Sy 1.5	100	2011 January 12	HIP 25143 (A3V)	5.14

[a]Redshift taken from the NASA/IPAC Extragalactic Database (NED).
[b]Apparent total J-band magnitude (in Vega), taken from 2MASS All-Sky Extended Source Catalog (Skrutskie et al. 2006).
[c]Activity classification is taken from Véron-Cetty & Véron (2010) unless a remark is given.
[d]Spectral type of each standard star is given in the parenthesis.
[e]Apparent J-band magnitude (in Vega) taken from 2MASS All-Sky Catalog of Point Sources (Cutri et al. 2003).
[f]Boselli et al. (2014).

3. RESULTS

The fully reduced spectra of the 26 Seyfert galaxies are shown in Figure 1. Here the flux scale is normalized by the flux density of the continuum emission at $\lambda_{\rm rest} = 1.235\mu$m. The [P II] emission is significantly detected in 6 objects (NGC 5506, Mrk 3, Mrk 6, Mrk 477, Mrk 1073, and MCG +08-11-011) among the 26 targets, while 19 objects show the significant [Fe II] emission. The Paβ emission is also detected in 11 objects, but we do not measure the emission-line properties of Paβ for Mrk 6 and MCG +08-11-011 because of their very complex spectral profiles. The measured central wavelength and velocity width in FWHM for each detected emission line are given in Table 2, and the derived flux ratios of [Fe II]/[P II] and [Fe II]/Paβ are given in Table 3. The averages and standard deviations of velocity width of detected emission lines are 717 ± 265 km s^{-1}, 596 ± 337 km s^{-1}, and 497 ± 321 km s^{-1} (for [P II], [Fe II], and Paβ, respectively) in FWHM.

In addition to the results obtained in our observations, we also collected flux ratios of [Fe II]/[P II] and [Fe II]/Paβ from the literature in order to expand the sample size to enable a better statistical analyses of the flux ratios. The compiled flux ratios for 23 objects are summarized in Table 4.

Figure 2 shows the histograms of the measured [Fe II]/[P II] flux ratio or its lower limit of the objects observed in our OAO observations and also compiled from the literature. The averages and standard deviations of the [Fe II]/[P II] flux ratio for [P II]-detected objects in our OAO sample and in the sample from the literature are 4.24 ± 1.47 and 2.83 ± 1.15, respectively. Note that Mrk 766 is included in both our OAO sample and also the sample compiled from the literature, and both of the two independent data of Mrk 766 are shown in Figure 2. Specifically, Schönell et al. (2014) reported that [Fe II]/[P II] = 2.654±0.164, that is consistent with our result ([Fe II]/[P II] > 2.483). Hereinafter we adopt the flux ratio reported by Schönell et al. (2014) for Mrk 766. Mrk 34 is also included in our sample and in the sample from the literature; we adopt the flux ratio reported by Jackson & Beswick (2007) since our OAO observation did not detect any emission lines (see Figure 1). Our OAO observations show the presence of many nearby AGNs with lower limits of [Fe II]/[P II] flux ratios, that have not been often reported in the literature. This may be partly because the lower limit of the [Fe II]/[P II] flux ratio for [P II]-undetected objects has been unreported in the literature.

Figure 3 shows the histograms of the measured [Fe II]/[P II] flux ratio or its lower limit for each AGN

TABLE 2
DETECTED EMISSION LINES[a]

name	[P II] 1.188μm		[Fe II] 1.257μm		Paβ[b] 1.282μm	
	λ_{obs}	FWHM	λ_{obs}	FWHM	λ_{obs}	FWHM
NGC 1667	–	–	1.2763	164	–	–
NGC 2273	–	–	1.2648	354	1.2897	258
NGC 2782	–	–	1.2681	300	1.2933	200
NGC 3079	–	–	1.2611	446	–	–
NGC 3982	–	–	–	–	–	–
NGC 4102	–	–	1.2603	229	1.2855	175
NGC 4169	–	–	–	–	–	–
NGC 4192	–	–	–	–	–	–
NGC 4258	–	–	–	–	–	–
NGC 4388	–	–	1.2566	511	1.2926	324
NGC 4419	–	–	1.2561	301	1.2812	511
NGC 4941	–	–	1.2616	475	1.2865	233
NGC 5005	–	–	1.2604	1251	–	–
NGC 5194	–	–	1.2587	548	–	–
NGC 5506	1.1957	340	1.2644	468	1.2900	808
NGC 6500	–	–	1.2696	474	–	–
NGC 6951	–	–	–	–	–	–
Mrk 3	1.2045	1050	1.2737	1091	1.2989	1072
Mrk 6	1.2113	1017	1.2797	1062	– [c]	– [c]
Mrk 34	–	–	–	–	– [d]	– [d]
Mrk 463	–	–	1.3199	1212	– [d]	– [d]
Mrk 477	1.2333	480	1.3042	691	– [d]	– [d]
Mrk 509	–	–	–	–	– [d]	– [d]
Mrk 766	–	–	1.2729	276	1.2984	888
Mrk 1073	1.2160	605	1.2859	470	– [d]	– [d]
MCG +08-11-011	1.2127	812	1.2821	957	– [c]	– [c]

[a]Observed central wavelength (μm) and FWHM (km s^{-1}) where the latter is corrected for the instrumental broadening.
[b]Narrow component.
[c]Not measured due to complex spectral features.
[d]Out of the wavelength coverage in our observations.

TABLE 3
EMISSION-LINE FLUX RATIOS OF THE TARGETS

Name	[Fe II]/[P II]	[Fe II]/Paβ
NGC 1667	> 3.174	> 3.064
NGC 2273	> 5.406	0.876±0.086
NGC 2782	> 15.88	1.218±0.019
NGC 3079	> 4.481	> 4.048
NGC 4102	> 7.427	0.627±0.021
NGC 4388	> 5.896	0.614±0.038
NGC 4419	> 4.067	1.242±0.118
NGC 4941	> 4.880	1.525±0.155
NGC 5005	> 12.37	> 12.31
NGC 5194	> 3.512	> 6.660
NGC 5506	6.876±0.645	0.278±0.003
NGC 6500	> 4.349	> 8.259
Mrk 3	3.974±0.162	1.314±0.023
Mrk 6	3.508±0.245	– [a]
Mrk 463	> 17.46	– [b]
Mrk 477	4.330±0.414	– [b]
Mrk 766	> 2.280	0.071±0.007
Mrk 1073	2.460±0.168	– [b]
MCG +08-11-011	4.256±0.220	– [a]

NOTE. — 3σ lower limits.
[a]Not measured due to complex spectral features.
[b]Paβ is out of the wavelength coverage in our observations.

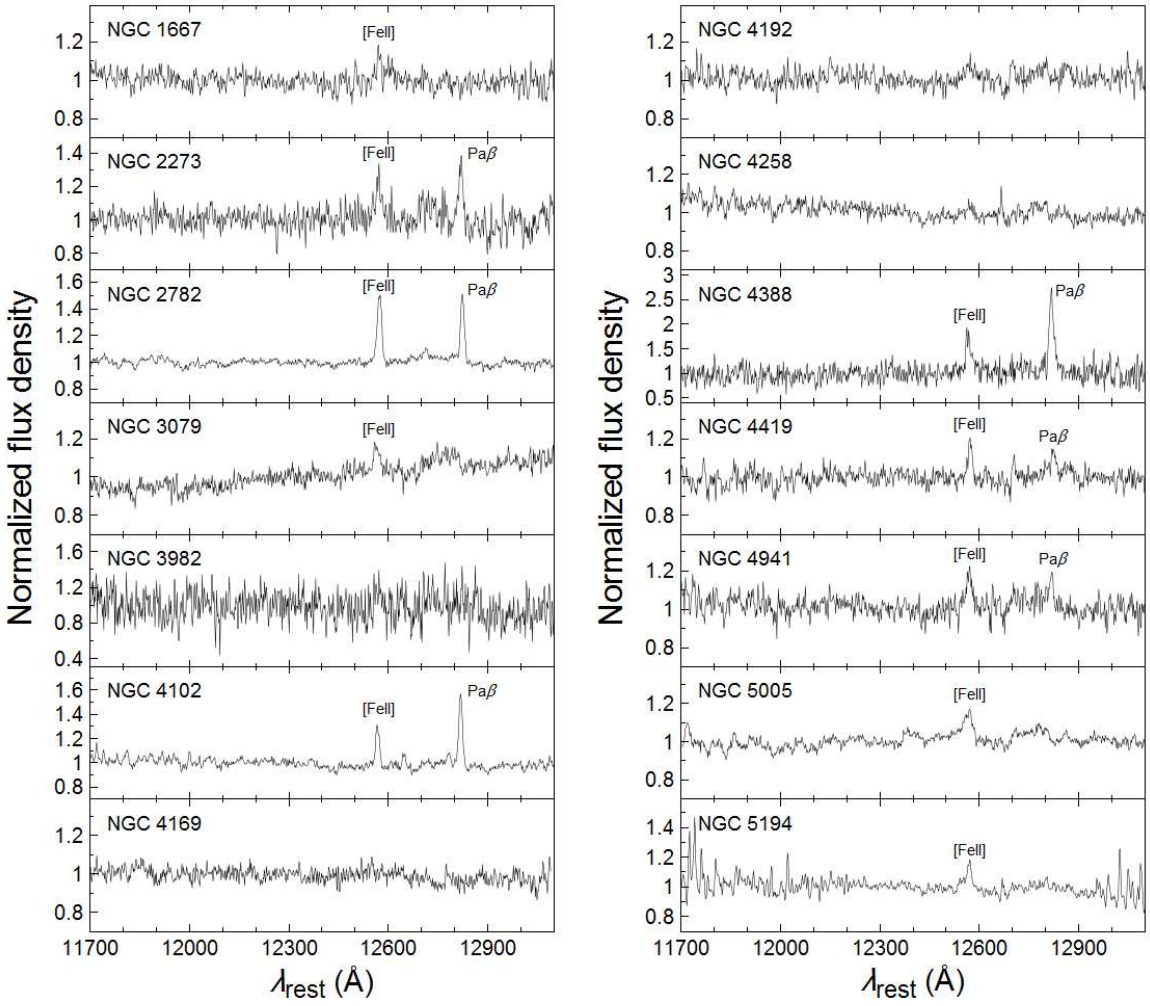

FIG. 1.— Rest-frame J-band spectra of our sample galaxies. Flux density is normalized to the 1.235μm continuum level.

TABLE 4
Emission-line flux ratios in the literature

Name	z[a]	[Fe II]/[P II]	[Fe II]/Paβ	Type[b]	Ref[c]
NGC 34	0.0196	1.55±0.43	1.07±0.14	Sy 2	1
NGC 1068	0.0038	1.33±0.06	0.46±0.02	Sy 2	2
NGC 1275	0.0176	3.35±0.12	1.05±0.06	Sy 1.5	1
NGC 2110	0.0078	5.61±1.07	5.45±0.32	Sy 2	1
NGC 3227	0.0039	2.80±0.61	1.21±0.08	Sy 1.5	1
NGC 4151	0.0033	2.98±0.21	0.54±0.03	Sy 1.5	1
NGC 5128	0.0018	3.0[d]	2.3[d]	FR I[e]	3
NGC 5929	0.0083	4.3±1.1	– [f]	LINER	4
NGC 7212	0.0266	3.64±0.42	0.86±0.05	Sy 2	5
NGC 7465	0.0065	>3.42[g]	1.28±0.34	LINER	5
NGC 7469	0.0163	1.76±0.27	0.39±0.03	Sy 1.5	1
NGC 7674	0.0289	1.90±0.19	1.04±0.11	Sy 2	1
Mrk 34	0.0505	3.2±1.0	– [f]	Sy 2	4
Mrk 78	0.0372	1.82±0.39	0.55±0.11	Sy 2	6
Mrk 79	0.0222	1.55±0.67	0.17±0.05	Sy 1	7
Mrk 334	0.0219	2.17±0.47	0.58±0.03	Sy 1.8	1
Mrk 348	0.0150	4.14±0.67	0.99±0.10	Sy 2	5
Mrk 573	0.0172	5.00±1.07	1.08±0.11	Sy 2	5
Mrk 766	0.0129	2.65±0.16	0.38±0.03	Sy 1	8
Mrk 1066	0.0120	2.74±0.24	0.79±0.03	Sy 2	5
Mrk 1157	0.0152	2.63±0.31	0.82±0.07	Sy 2	9
Ark 564	0.0247	2.07±0.40	0.09±0.01	LINER	1
ESO 428−G014	0.0057	1.99±0.11	0.67±0.02	Sy 2	1

[a]Redshift taken from the NASA/IPAC Extragalactic Database (NED).
[b]Activity classification is taken from Véron-Cetty & Véron (2010) unless a remark is given.
[c]References: (1) Riffel et al. (2006); (2) Hashimoto et al. (2011); (3) Krajnović et al. (2007); (4) Jackson & Beswick (2007); (5) Ramos Almeida et al. (2009); (6) Ramos Almeida et al. (2006); (7) Riffel et al. (2013); (8) Schönell et al. (2014); (9) Riffel & Storchi-Bergmann (2011).
[d]The error of the flux ratio is not given in the literature.
[e]Hardcastle et al. (2003).
[f]Not available in the literature.
[g]3σ lower limit.

type. The averages and standard deviations of the [Fe II]/[P II] flux ratio for [P II]-detected un-obscured (i.e., type 1 and type 1.5) Seyfert galaxies (9 objects) and obscured (i.e., type 2) Seyfert galaxies (16 objects) are 2.78 ± 0.82 and 3.32 ± 1.53, respectively. Though there may be a tendency that objects showing a large [Fe II]/[P II] flux ratio are in the Seyfert 2 and LINER samples, we cannot conclude it statistically because of small sample sizes in this work. Note that a Fanaroff-Riley type I (FR I) galaxy, NGC 5128, shows a moderate value of the [Fe II]/[P II] flux ratio (∼3.0; see Table 4), despite the presence of a radio jet. We will discuss the implication for the relation between the radio jet and the ionization mechanism of the NLR gas clouds inferred from the measured [Fe II]/[P II] flux ratio in Section 4.2.

4. DISCUSSION

4.1. *Emission-line flux ratios of the targets*

As shown in the previous section, we measured the flux ratio of [Fe II]/[P II] for 6 objects with [P II] detection in our OAO sample and collected 22 objects from the literature, accordingly for a total of 28 [P II]-detected objects. The average and standard deviation of this flux ratio for the 28 [P II]-detected objects are 3.13 ± 1.33, and the median value is 2.88 (see also Tables 3 and 4). This is roughly consistent with the prediction of photoionization models, that expect ∼2 for the [Fe II]/[P II] ratio (e.g., Oliva et al. 2001). On the other hand, some objects show a much higher ratio of [Fe II]/[P II], reaching at ∼10 or even more. As demonstrated by Oliva et al. (2001), such a high [Fe II]/[P II] ratio suggests a significant contribution of fast shocks in the ionization of NLR gas clouds. It is therefore concluded that shock-dominated NLRs actually exist, at least in some NLRs of AGNs in the nearby Universe.

Some previous long-slit and integral-field unit (IFU) observations show the spatial variation of the [Fe II]/[P II] flux ratio in some nearby Seyfert galaxies, in the sense that the [Fe II]/[P II] flux ratio increases as a function of the distance from the nucleus (e.g., Storchi-Bergmann et al. 2009; Riffel et al. 2010; Hashimoto et al. 2011). The flux ratio reaches up to ∼10 at the outer part of NLRs in NGC 4151 (Storchi-Bergmann et al. 2009) and Mrk 1066 (Riffel et al. 2010), suggesting that the shock contribution could be much more significant at the outer part than the inner part of NLRs. This trend is a natural consequence of the geometrical dilution of ionizing photons from the nucleus (see also, e.g., Jackson & Beswick 2007). However, the surface emissivity of emission lines at the outer part of NLRs is much lower than the inner part of NLRs generally, and thus the integrated NLR spectrum of AGNs does not necessarily show shock-dominated line-flux ratios even if the outer part of NLRs shows such a high [Fe II]/[P II] flux ratio. Our OAO/ISLE spectra are extracted at the nuclear 2″.0 region, and the extracted spectra should not be dominated by the outer part of the NLR in the target AGNs. For exam-

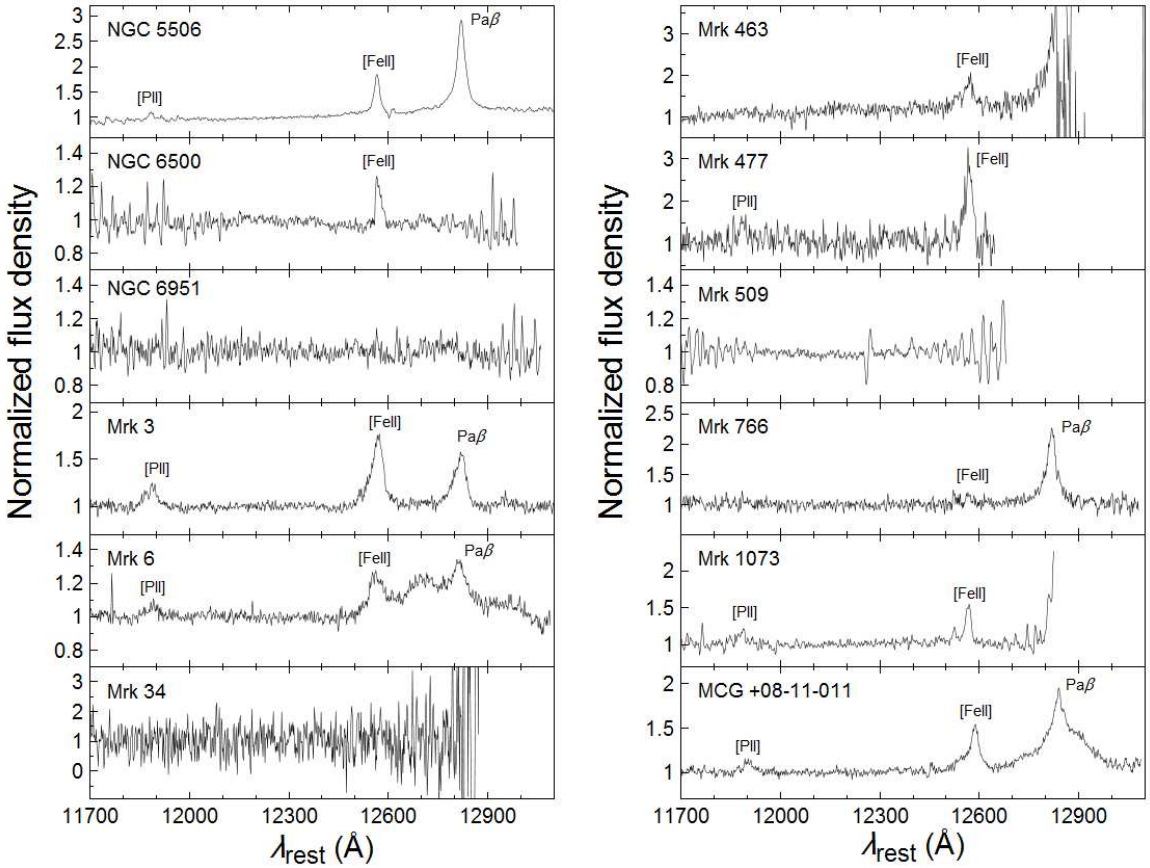

FIG. 1.— (Continued.)

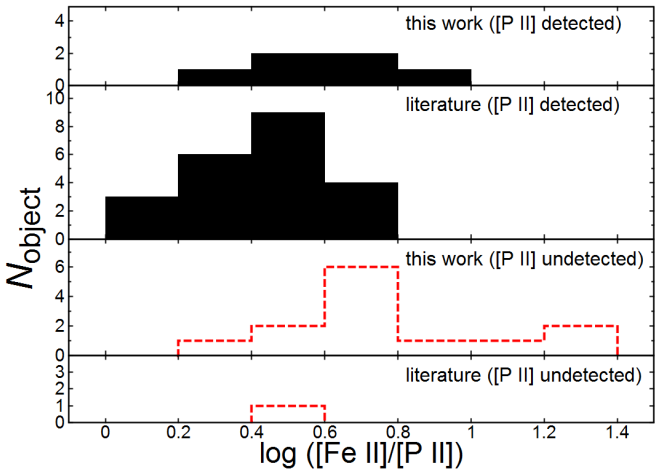

FIG. 2.— Histograms for our sample and the compiled one. Filled-black histograms denote [P II]-detected data while red-dashed histograms denote [P II]-undetected data. The data of [P II]-detected objects in our OAO sample, [P II]-undetected objects in our OAO sample, [P II]-detected objects in the literature, and [P II]-undetected objects in the literature, are shown from the top to the bottom panel. For the [P II]-detected objects, 3σ lower limit of the [Fe II]/[P II] flux ratio is shown.

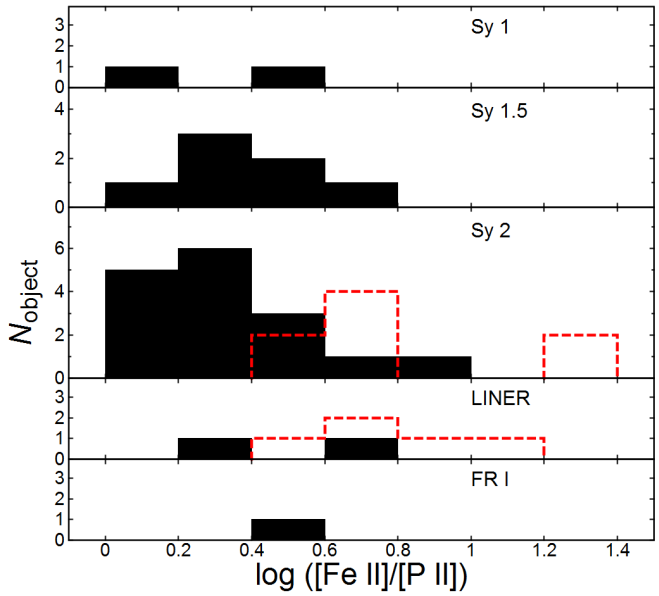

FIG. 3.— Same as Figure 2 but for each AGN type. The type 1 Seyfert galaxies, type 1.5 Seyfert galaxies (including type 1.8 Seyfert galaxies), type 2 Seyfert galaxies, LINERs, and FR I radio galaxies, are shown from the top to the bottom panel, respectively. The filled-black and red-dashed histograms are the same as in Figure 2.

ining whether our OAO targets with a high flux ratio of [Fe II]/[P II] are affected by such a possible aperture effect or not, we show the relation between the measured [Fe II]/[P II] flux ratio and the physical scale covered by the aperture size ($= 2''.0$) at the target redshift in Figure 4. Though a positive correlation between the measured [Fe II]/[P II] flux ratio and the physical scale covered by the adopted aperture is expected if the high [Fe II]/[P II] flux ratio seen in our sample is caused by the significant contribution of the outer part of NLRs, Figure 4 does not show such a significant positive correlation. This suggests that the high [Fe II]/[P II] flux ratio seen in some objects in our OAO sample is not due to the geometrically-diluted ionizing photons at the outer part of NLRs.

It has been reported that the enhancement of the [Fe II]/Pa β flux ratio is seen in shock-excited regions, not only the [Fe II]/[P II] flux ratio (e.g., Larkin et al. 1998; Mouri et al. 2000; Ramos Almeida et al. 2009; Koo & Lee 2015), that is due mostly to the destruction of dust grains by fast shocks. Figure 5 shows the clear positive correlation between the [Fe II]/[P II] and [Fe II]/Pa β flux ratios, i.e., objects showing a large [Fe II]/[P II] ratio also show a large [Fe II]/Pa β ratio. This positive correlation has been reported by Ramos Almeida et al. (2009) for a smaller sample (6 Seyfert galaxies), but now the correlation is shown for a much larger sample in this work. This supports the interpretation that a large [Fe II]/[P II] ratio seen in NLRs of some AGNs is caused by fast shocks.

Note that, at high ionization parameter where Compton heating becomes significant, the photoionization may also destroy dust grains, resulting in higher [Fe II]/[P II] ratios without fast shocks. Such objects should be distinguished by checking the relative strength of coronal forbidden lines. In order to examine this possibility, we investigate the relative strength of coronal forbidden lines in our samples. We find the [Fe VII]λ6087/[O III]λ5007 flux ratio for 21 objects (20 [P II]-detected and 1 [P II]-undetected objects) from the literature (Nagao et al. 2000, 2003; Bennert et al. 2006). Note that this flux ratio is very sensitive to the ionization parameter, in the sense that a higher [Fe VII]λ6087/[O III]λ5007 flux ratio is achieved by a higher ionization parameter (see, e.g., Figure 13 in Nagao et al. 2001). We also focus on a mid-infrared coronal line of [Ne V]14.32μm, and compile the [Ne V]14.32μm/[Ne II]12.81μm flux ratio for 24 objects (17 [P II]-detected and 7 [P II]-undetected objects) from the literature (Pereira-Santaella et al. 2010; Weaver et al. 2010; Wu et al. 2011; Petric et al. 2011; Dasyra et al. 2011). Figures 6 and 7 show the relation between the [Fe II]/[P II] flux ratio and the relative strength of two coronal forbidden lines. Though we expect a positive correlation in these figures if high-ionization gas clouds without fast shocks result in high [Fe II]/[P II] flux ratios, we do not see such a trend in both figures. These results further support our conclusion that a large [Fe II]/[P II] flux ratio seen in our samples is due to fast shocks, not to the photoionization with a very high ionization parameter.

4.2. *Relation between the emission-line flux ratio and radio loudness*

As described already, large [Fe II]/[P II] ratios seen in some AGNs are attributed by fast shocks in NLRs. The most simple idea for the origin of the fast shocks in NLRs is the effect of the AGN jet. Previous radio observations show that AGN jets exist not only in powerful radio galaxies; actually less-powerful radio jets are seen in many radio-quiet AGNs such as Seyfert galaxies, with much smaller spatial extension than seen in powerful radio galaxies (e.g., Miller et al. 1993; Ulvestad et al. 1999; Nagar et al. 2001). Therefore, such AGN jets including small-scale weak jets may cause fast shocks in NLRs and then the gas-phase iron abundance increases through the

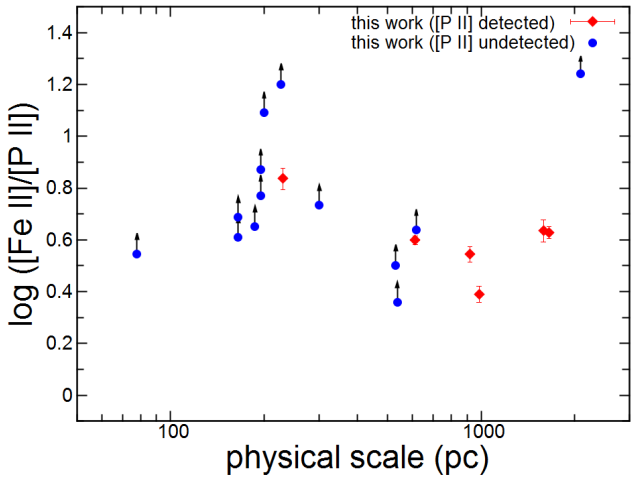

FIG. 4.— Relation between the measured [Fe II]/[P II] flux ratio and the physical scale covered by the aperture size (= 2″.0) at the target redshift. Red diamonds and blue circles denote [P II]-detected and [P II]-undetected objects in our OAO sample, respectively. For the [P II]-undetected objects, the 3σ lower limit of the [Fe II]/[P II] flux ratio is shown.

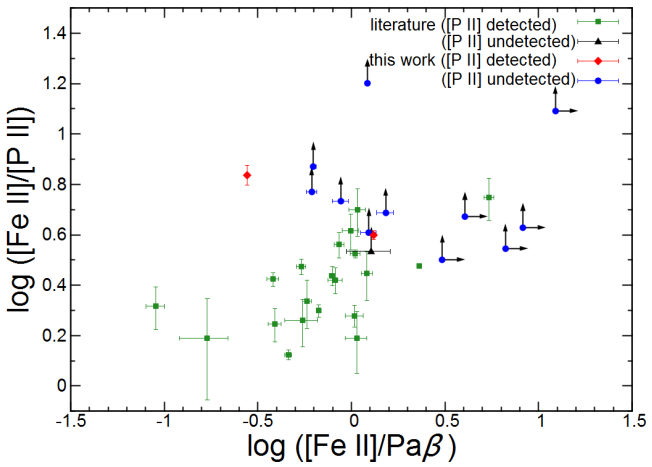

FIG. 5.— Relation between the [Fe II]/[P II] and [Fe II]/Paβ flux ratios. Red diamonds and blue circles are the same as in Figure 4, while green squares and black triangles denote [P II]-detected and [P II]-undetected objects in the sample from the literature. Arrows denote 3σ limits on the emission-line flux ratio.

grain destruction or the sputtering process, resulting in a large [Fe II]/[P II] ratio observed in some AGNs.

For examining whether the observed large [Fe II]/[P II] ratio seen in some AGNs is actually attributed to the AGN jet or not, the most straightforward test is to investigate the relation between the [Fe II]/[P II] ratio and the power of the AGN jet. For quantifying the power of the AGN jet, we adopt the radio loudness (R) that is defined as the ratio of the flux density of the radio (5 GHz) to the optical (4400 Å), i.e.,

$$R = \frac{\text{5 GHz flux density}}{\text{4400 Å flux density}} \quad (1)$$

(Kellermann et al. 1989). In this definition, AGNs are classified as radio-loud and radio-quiet populations at the threshold of $R = 10$ (Kellermann et al. 1989). We calculate the radio loudness by compiling the optical and

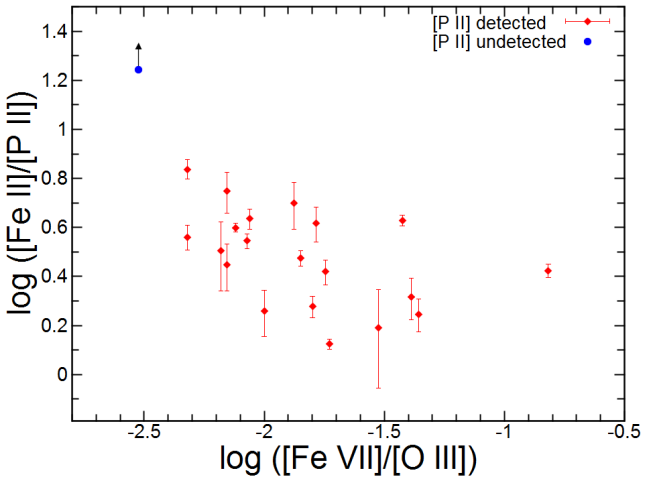

FIG. 6.— Relation between the [Fe II]/[P II] and the [Fe VII]λ6087/[O III]λ5007 flux ratios. Red diamonds and blue circles denote [P II]-detected and [P II]-undetected objects, respectively. Arrows denote 3σ limits on the emission-line flux ratio.

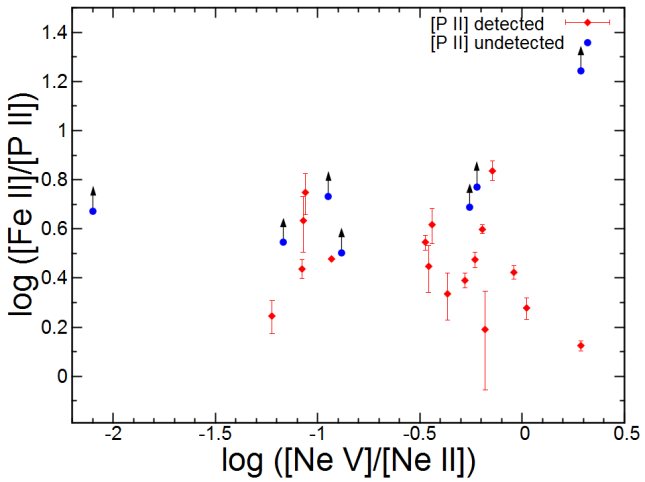

FIG. 7.— Relation between the [Fe II]/[P II] and the [Ne V]14.32μm/[Ne II]12.81μm flux ratios. Symbols are the same as in Figure 6.

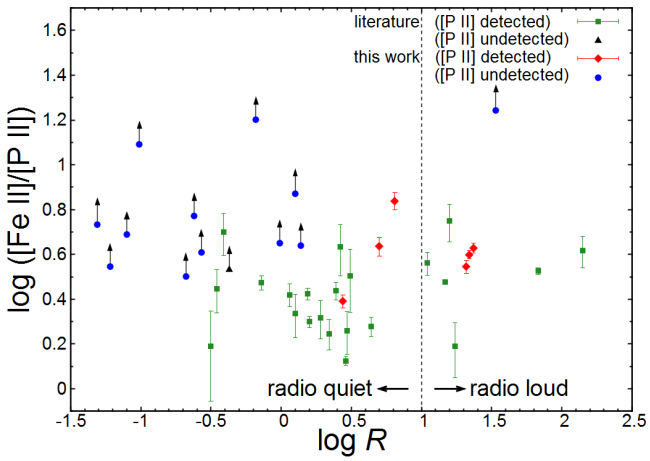

FIG. 8.— Relation between the [Fe II]/[P II] flux ratio and the radio-loudness (R). Symbols are the same as in Figure 5. Perpendicular dashed line shows the threshold dividing the radio-loud and radio-quiet populations.

radio flux densities from previous observations, for both our OAO sample and the sample from the literature. For the cases that multiple photometric data are available, we use the data whose aperture size is as small as possible for avoiding any contributions from the host galaxy. From the compiled photometric data, we derive the flux density at 5 GHz and 4400 Å by adopting the typical spectral index of Seyfert galaxies, i.e., −0.5 (optical) and −0.7 (radio) respectively (Singh et al. 2015).

Figure 8 shows the [Fe II]/[P II] flux ratio as a function of the radio loudness, in the logarithmic scale. There is no apparent positive or negative correlation between the [Fe II]/[P II] flux ratio and the radio loudness. For the [P II]-detected objects, there is no statistically significant difference in the average value of the [Fe II]/[P II] flux ratio between the radio-loud and radio-quiet populations; 3.67 ± 1.09 for 9 objects with $R > 10$ (i.e., radio-loud, including NGC 5128 that is a FR I radio galaxy) while 2.87 $\pm$ 1.38 for 19 objects with $R < 10$ (i.e., radio-quiet). We thus conclude that the [Fe II]/[P II] flux ratio is not determined primarily by the AGN jet. Note that this conclusion does not change even when the [P II]-undetected objects are taken into account, because there is only 1 [P II]-undetected (Mrk 463) in the radio-loud domain in our samples. This result strongly suggests that the radio jet is not the main origin of fast shocks in NLRs of AGNs.

4.3. *Relation between the emission-line flux ratio and kinematics*

As described in Section 1, the [Fe II] and [P II] emission lines arise at similar locations in the NLR due to the similarity of the critical density and ionization potential. Therefore, the velocity profiles of these two lines are expected to be similar in each other. However, NLR clouds affected by fast shocks may be kinematically disturbed. Therefore the velocity profile of [Fe II] and [P II] emission lines may tell us some hints about the contribution of fast shocks in NLRs. Figure 9 shows the relation between the [Fe II]/[P II] flux ratio and the FWHM ratio of [Fe II] and [P II], and we see a significant positive correlation between the two quantities. Specifically, AGNs showing a larger [Fe II]/[P II] flux ratio tend to show wider [Fe II] velocity profile with respect to the [P II] velocity profile. The linear fit to this correlation results in the relation of

$$\text{[Fe II]/[P II]} = (4.690 \pm 1.866) \times \frac{\text{FWHM}_{\text{[Fe II]}}}{\text{FWHM}_{\text{[P II]}}} + (-1.128 \pm 2.174) \quad (2)$$

(see Figure 9). Note that this positive correlation is not expected if all of the observed flux of the [Fe II] and [P II] emission lines comes from NLR clouds excited by fast shocks, because in this case both [Fe II] and [P II] velocity profiles should be disturbed similarly by the shock and thus the FWHM ratio is expected to be ∼1. The observed correlation shown in Figure 9 is explained by the mixture of the photoionized cloud and shock-excited cloud in NLRs. More specifically, the [Fe II] flux of AGNs with a large [Fe II]/[P II] flux ratio is significantly attributed by fast shocks while the [P II] flux is largely attributed by photoionized clouds in the NLR. This picture is consistent to the fact that the observed [Fe II]/[P II] flux ratio does not reach up to the value expected by pure shocks (∼20).

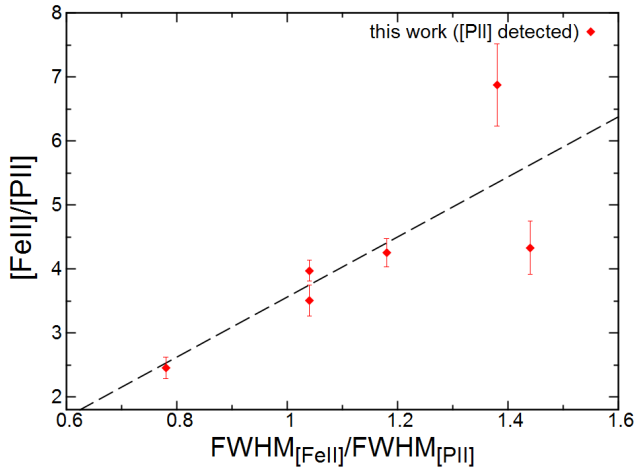

FIG. 9.— Relation between the [Fe II]/[P II] flux ratio and the FWHM ratio of [Fe II] and [P II] for objects whose [Fe II] and [P II] are detected in our OAO run. Dashed line represents the linear-fit result.

4.4. *Origin of the fast shock in NLRs*

As already described, our results show that the radio jet is not the primary origin of fast shocks in NLRs, at least low-z AGNs investigated in this work. Then, what is the origin of fast shocks in NLRs? Recently, powerful AGN-driven outflows are observed in some high-z (e.g., Maiolino et al. 2012; Carniani et al. 2015) and low-z AGNs (e.g., Rupke & Veilleux 2011; García-Burillo et al. 2014; Feruglio et al. 2015). The possible launching mechanisms of powerful AGN outflows are the radiation pressure from the UV photons and/or line-force (e.g., Murray et al. 1995; Binette et al. 1997; Proga et al. 2008; Nomura et al. 2016), thermally driven (e.g., Begelman et al. 1983; Krolik & Kriss 2001), magnetocentrifugal force due to an accretion disk (e.g., Blandford & Payne 1982; Konigl & Kartje 1994). Those outflows are characterized by broad (FWHM $\gtrsim$ 1000 km s^{-1}) and/or blueshifted emission lines, mostly extending up to the kpc scale. The opening angle of those outflows is much wider than that of radio jets generally, and such powerful outflows are seen not only in radio-loud AGNs. Therefore it is strongly suggested that the main driving source of those AGN outflows is not the radio jet. For example, Feruglio et al. (2015) reported the discovery of a molecular outflow spreading ∼1 kpc toward all directions from the nucleus of a type 1 Seyfert Mrk 231 (that is known also as an ultra-luminous infrared galaxy; ULIRG) based on CO(2-1) observations. The inferred mass-outflow rate and kinetic energy of the molecular outflow are $\dot{M} = 500 - 1000\ M_{\odot}\text{yr}^{-1}$ and $\dot{E}_{\rm kin} = 7 - 10 \times 10^{43}$ erg s^{-1} that corresponds to 1–2% of the AGN bolometric luminosity. Similarly, Cicone et al. (2014) reported the ratio of the kinetic energy of the outflow to the AGN bolometric luminosity in 14 low-z luminous AGNs (including ULIRGs) is up to 5%, also based on CO observations. The value of this ratio is close to predicted value from theoretical model for explaining the $M_{BH} - \sigma$ relation in local galaxies (e.g., Silk & Rees

TABLE 5
Various properties of our samples

Name	[Fe VII]/[O III]	Ref	[Ne V]/[Ne II]	Ref	$f_{5\mathrm{GHz}}$ (mJy)	Ref	f_{4400} (mJy)	Ref	log R	log L_{FIR} ($L_\odot$)	log $\nu L_\nu(K_\mathrm{s})$ ($L_\odot$)
objects observed at OAO											
NGC 1667	–		0.131	4	5.0	9	24.1±7.08	19	−0.68	10.55	10.38
NGC 2273	–		0.113	5	2.4	10	49.4±9.44	19	−1.31	10.00	10.05
NGC 2782	–		–		44.05	11	66.9±9.91	19	−0.18	9.89	9.65
NGC 3079	–		0.008	5	120.15	11	124±17.1	19	−0.01	10.47	10.12
NGC 3982	–		–		1.63	11	82.7±13.1	19	−1.71	9.80	9.59
NGC 4102	–		–		91.60	11	72.7±10.8	19	0.10	10.48	9.61
NGC 4169	–		–		0.59	11	23.0±4.14	19	−1.59	10.29	10.32
NGC 4192	–		–		6.88	11	222±21.4	19	−1.51	9.49	10.09
NGC 4258	–		–		2.43	11	819±121	19	−2.53	9.46	10.01
NGC 4388	–		0.600	5	18.46	11	76.1±5.82	19	−0.62	9.86	9.86
NGC 4419	–		–		16.20	11	60.5±4.62	19	−0.57	9.64	9.82
NGC 4941	–		0.554	5	4.92	11	61.6±14.5	19	−1.10	8.93	9.63
NGC 5005	–		–		18.78	11	191±30.4	19	−1.01	10.25	10.51
NGC 5194	–		0.068	5	6.04	11	994±147	19	−1.22	9.71	10.06
NGC 5506	0.0048	1	0.716	5	138.53	11	21.5±3.89	19	0.81	9.86	9.93
NGC 6500	–		–		35.8	10	25.7±4.91	19	0.14	9.86	10.40
NGC 6951	–		–		36±8	12	73.3±11.7	19	−0.31	10.17	10.19
Mrk 3	0.0076	1	0.640	5	355.59	13	16.2±2.75	19	1.34	10.33	10.47
Mrk 6	0.0085	1	0.336	5	98.5	13	4.76±0.76	19	1.32	10.12	10.59
Mrk 34	0.0066	1	–		7.91	11	2.56±0.71	20	0.49	10.73	10.49
Mrk 463	0.0030	2	1.935	5	150.81	11	4.42±0.85	19	1.53	11.14	11.09
Mrk 477	0.0087	1	–		24.28	11	4.89±1.35	20	0.70	10.75	10.07
Mrk 509	–		–		7.87±0.41	14	7.76±2.14	20	0.01	11.07	11.22
Mrk 766	0.1524	1	0.913	5	16.54	11	10.7±2.16	19	0.19	10.25	10.01
Mrk 1073	–		0.525	6	38.58±1.19	14	14.1±4.49	19	0.44	11.13	10.42
MCG +08-11-011	0.0376	1	–		100.90±3.57	14	4.26±0.86	21	1.37	11.13	11.26
objects from the literature											
NGC 34	–		–		44.39±5.79	15	2.58±0.01	22	1.24	11.24	10.28
NGC 1068	0.0187	1	1.941	5	1650.25	11	577±85.5	19	0.46	10.66	10.35
NGC 1275	–		–		3100±160	16	45.4±5.78	19	1.83	10.71	10.89
NGC 2110	0.0070	1	0.087	7	104.80±4.92	17	6.66±0.43	23	1.20	9.95	10.30
NGC 3227	0.0070	1	0.348	5	33.96	11	98.5±16.7	19	−0.46	9.85	10.08
NGC 4151	0.0142	1	0.588	5	135.83	11	186±27.6	19	−0.14	9.30	9.80
NGC 5128	–		0.117	5	52662±2662	18	3540±756	19	1.17	9.65	10.04
NGC 5929	–		0.085	5	28.95	11	10.92±0.29	24	0.42	10.35	10.05
NGC 7212	0.0048	3	–		42.29	11	3.89±1.73	25	1.04	10.84	10.51
NGC 7465	–		–		8.53±0.57	14	20.2±3.86	19	−0.37	9.61	9.51
NGC 7469	0.0440	1	0.060	5	59.73	11	27.4±3.77	19	0.34	11.27	10.58
NGC 7674	0.0159	1	1.050	5	72.48	11	16.7±3.18	19	0.64	10.78	10.37
Mrk 34	0.0066	1	–		7.91	11	2.56±0.71	20	0.49	10.73	10.49
Mrk 78	0.0100	1	–		17.37±3.86	15	5.88±1.63	20	0.47	10.62	10.38
Mrk 79	0.0299	1	0.660	5	6.09	11	19.3±3.69	19	−0.50	10.64	10.80
Mrk 334	–		0.433	4	9.65±3.86	15	7.68±1.38	19	0.10	10.82	10.36
Mrk 348	0.0165	1	0.363	5	801.7	9	5.72±1.16	19	2.15	9.99	10.07
Mrk 573	0.0133	1	–		5.64	11	14.4±2.13	19	−0.41	9.99	10.05
Mrk 766	0.1524	1	0.913	5	16.54	11	10.7±2.16	19	0.19	10.25	10.01
Mrk 1066	–		0.084	8	36.67±3.86	15	14.9±2.21	19	0.39	10.62	9.97
Mrk 1157	0.0180	1	–		13.65±0.45	14	11.8±2.14	19	0.06	10.17	10.08
Ark 564	0.041	1	–		11.93±0.41	14	6.26±1.48	19	0.28	10.23	10.22
ESO 428-G014	–		–		33.50±1.23	14	21.2±4.51	19	0.20	9.57	9.68

Note. — References: (1) Nagao et al. 2000; (2) Nagao et al. 2003; (3) Bennert et al. 2006; (4) Wu et al. 2011; (5) Pereira-Santaella et al. 2010; (6) Petric et al. 2011; (7) Weaver et al. 2010; (8) Dasyra et al. 2011; (9) Gallimore et al. 2006; (10) 1.4 GHz data from Nagar et al. 2005; (11) FIRST catalog (*Faint Images of the Radio Sky at Twenty-cm*); (12) Sramek 1975; (13) 4.89 GHz data from Laurent-Muehleisen et al. 1997; (14) 1.4 GHz data from Condon et al. 1998; (15) Bicay et al. 1995; (16) Taylor et al. 2006; (17) 4.89 GHz data from Ulvestad & Wilson 1984; (18) 4.85 GHz data from Gregory et al. 1994; (19) de Vaucouleurs et al. 1991, RC3 (*Third Reference Catalog of Bright Galaxies*), photographic magnitude; (20) 4680 Å data from Petrosian et al. 2007; (21) de Vaucouleurs et al. 1991 (RC3), total magnitude; (22) Schweizer & Seitzer 2007; (23) 4480 Å data from McAlary et al. 1983; (24) SDSS, g-band (4860 Å); (25) Zwicky & Kowal 1968, CGCG (*Catalogue of Galaxies and Clusters of Galaxies*).

1998; King 2010). Therefore, it is likely that powerful AGN-driven outflows can give impacts on NLR clouds and consequently cause fast shocks in NLRs.

However, the physical origin of such powerful AGN-driven outflows in the galactic scale is also unknown. At a smaller spatial scale in AGNs, powerful outflows are sometimes recognized as the BAL and UFO. Since BAL features are seen in rest-frame UV spectra and thus they are observed mainly for high-z quasars (e.g., Weymann et al. 1991), we here focus on the UFO that are seen in rest-frame hard X-ray spectra of nearby AGNs (e.g., Tombesi et al. 2010). Specifically, the UFO is identified as a blue-shifted Fe K absorption line, whose outflowing velocity reaches mildly relativistic values (> 0.033c). Based on hydrodynamical simulations, Wagner et al. (2013) showed that the uncollimated UFO from the central engine of AGNs gives strong feedback effects into the ISM in the host galaxy at the kpc scale, similar to well-collimated radio jets (see, e.g., Wagner et al. 2012). Among our sample, 5 objects (NGC 4151, NGC 5506, Mrk 79, Mrk 509, and Mrk 766) show the UFO feature in their X-ray spectra (Tombesi et al. 2010; Gofford et al. 2013). These objects show relatively low [Fe II]/[P II] flux ratios that reach only up to $\sim$3, except for NGC 5506 (6.876$\pm$0.487) and Mrk 509 (unmeasured). This may suggest that AGNs with a shock-excited NLR are not necessarily associated with the UFO feature in their X-ray spectra. Here it should be noted that the UFO could be still important as a possible origin of fast shocks in NLRs, because AGNs without UFO features may possess powerful nuclear outflows that are not recognized as UFOs due to various effects such as the viewing-angle effect and obscuration effect. A larger sample of AGNs with the measurement of the [Fe II]/[P II] flux ratio and hard X-ray spectra is needed to investigate possible link between the fast shock in NLRs and the UFO phenomenon.

Moreover, we discuss another possible candidate for the origin of fast shocks, that is the wind originated from the nuclear starburst (e.g., Heckman et al. 1990; Rich et al. 2010; Ho et al. 2014, 2016). In order to examine whether the starburst is the main origin of the fast shock in the NLR or not, we investigate two indicators of the starburst activity. First, we focus on the far-infrared luminosity ($L_{\rm FIR}$), that is a tracer of the starburst activity in galaxies. We adopt the following definition of the far-infrared flux ($F_{\rm FIR}$) to derive $L_{\rm FIR}$,

$$F_{\rm FIR} = 1.26 \times 10^{-11}(2.58S_{60\mu{\rm m}} + S_{100\mu{\rm m}}) \qquad (3)$$

where $S_{60\mu{\rm m}}$ and $S_{100\mu{\rm m}}$ are the *IRAS* flux densities in Jy at 60μm and 100μm, respectively (Fullmer & Londsdale 1989; Sanders & Mirabel 1996), and $F_{\rm FIR}$ is given in unit of erg s^{-1} cm^{-2}. Since the outflow due to the starburst is determined by both the starburst activity and the depth of the gravitational potential of galaxies, we investigate the far-infrared luminosity normalized by the $K_{\rm s}$-band luminosity ($\nu L_\nu(K_{\rm s})$), where the latter is derived by the total $K_{\rm s}$ magnitude taken from the 2MASS All-Sky Extended Source Catalog (Skrutskie et al. 2006). Figure 10 shows the relation between the [Fe II]/[P II] flux ratio and $L_{\rm FIR}/\nu L_\nu(K_{\rm s})$, and we find no significant positive correlation. This suggests that the large [Fe II]/[P II] flux ratio is not caused by the starburst activity in host galaxies

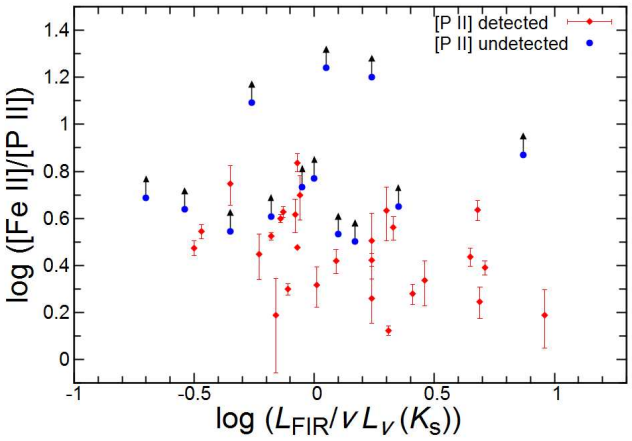

FIG. 10.— Relation between the [Fe II]/[P II] flux ratio and the far-infrared luminosity normalized to the $K_{\rm s}$ luminosity. Symbols are the same as in Figure 6.

of Seyfert galaxies. Second, we checked the 3.3μm polycyclic aromatic hydrocarbon (PAH) feature which is indicator of the nuclear starburst (e.g., Imanishi & Dudley 2000; Imanishi & Wada 2004). Since the strong PAH emission is expected for starburst galaxies while the PAH is destroyed in pure AGNs, we can infer the relative strength of the starburst to the AGN through the PAH emission. We collected the 3.3μm PAH data from the literature (Rodríguez-Ardila & Viegas 2003; Watabe et al. 2008; Oi et al. 2010; Castro et al. 2014). The averages and standard deviations of the [Fe II]/[P II] flux ratio for the PAH detected objects (7 objects) and undetected (upper limit) objects (6 objects) in [P II]-detected sample are 3.28$\pm$1.75 and 3.52$\pm$1.04, respectively. Since there is no systematic difference in the [Fe II]/[P II] flux ratio between the PAH-detected and PAH-undetected samples, the contribution of starburst-driven shocks to the [Fe II]/[P II] flux ratio appears to be negligible. Therefore, based on the two tracers of the starburst, $L_{\rm FIR}$ and PAH, we conclude that the starburst is not the primary origin of fast shocks in NLRs.

5. CONCLUSION

In order to investigate how the fast shock contributes to the NLR ionization, we have carried out near-infrared J-band spectroscopic observations of 26 nearby AGNs. In our analysis, we use the [Fe II]/[P II] flux ratio as a powerful diagnostics of the fast shock in the NLR. Among the 26 observed AGNs, the [P II] emission is significantly detected in 6 AGNs while the [Fe II] emission is significantly detected in 19 AGNs. By adding the data from the literature, we gather the [Fe II]/[P II] flux ratio or its lower limit for 23 nearby AGNs. Based on this combined large sample of Seyfert galaxies, we obtain the following results and conclusions.

1. We find that the [Fe II]/[P II] flux ratio in more than half of Seyfert galaxies in our sample are consistent to the prediction by the photoionization model ($\sim$2). However, the three Seyfert galaxies, NGC 2782, 5005, and Mrk 463 show very large [Fe II]/[P II] flux ratios ($\gtrsim$10), suggesting a significant contribution of the fast shock in the NLR excitation.

2. The positive correlation between the [Fe II]/[P II] flux ratio and the [Fe II]/Pa β reported in the literature is confirmed in our large sample of Seyfert galaxies. This also supports the interpretation that the NLR in AGNs with a large [Fe II]/[P II] flux ratio is affected by fast shocks.

3. The positive correlation between the [Fe II]/[P II] flux ratio and the FWHM ratio of [Fe II] and [P II] is found in our sample. This is consistent with the interpretation that the observed [Fe II] flux in AGNs with a large [Fe II]/[P II] flux ratio is significantly attributed by shock-excited clouds.

4. The [Fe II]/[P II] flux ratio in our sample shows no clear correlation with the radio loudness nor the strength of the starburst, suggesting that the radio jet and the starburst are not the primary origin of the fast shocks in the NLR.

This paper is based on observations with the 188 cm telescope at the Okayama Astrophysical Observatory (OAO) operated by National Astronomical Observatory of Japan (NAOJ). We thank K. Matsubayashi, T. Hori, N. Araki, and the OAO staffs for their support during the observations. We would like to thank the anonymous referee for her/his useful comments and suggestions that improved this paper very much. This work was financially supported in part by the Japan Society for the Promotion of Science (JSPS; TN: grant No. 25707010, 16H01101, and 16H03958; YT: 23244031 and 16H02166), and also by the JGC-S Scholarship Foundation. KM is financially supported by the JSPS through the JSPS Research Fellowship. This research has made use of the NASA/IPAC Extragalactic Database (NED) which is operated by the Jet Propulsion Laboratory, California Institute of Technology, under contract with the National Aeronautics and Space Administration. This publication makes use of data products from the Two Micron All Sky Survey, which is a joint project of the University of Massachusetts and the Infrared Processing and Analysis Center/California Institute of Technology, funded by the National Aeronautics and Space Administration and the National Science Foundation. IRAF is distributed by the National Optical Astronomy Observatory, which is operated by the Association of Universities for Research in Astronomy (AURA) under a cooperative agreement with the National Science Foundation.

REFERENCES

Allen, M. G., Groves, B. A., Dopita, M. A., Sutherland, R. S., & Kewley, L. J. 2008, ApJS, 178, 20
Begelman, M. C., McKee, C. F., & Shields, G. A. 1983, ApJ, 271, 70
Bennert, N., Jungwiert, B., Komossa, S., Haas, M., & Chini, R. 2006, A&A, 456, 953
Bicay, M. D., Kojoian, G., Seal, J., Dickinson, D. F., & Malkan, M. A. 1995, ApJS, 98, 369
Bicknell, G. V., Dopita, M. A., Tsvetanov, Z. I., & Sutherland, R. S. 1998, ApJ, 495, 680
Binette, L., Wilson, A. S., Raga, A., & Storchi-Bergmann, T. 1997, A&A, 327, 909
Binette, L., Wilson, A. S., & Storchi-Bergmann, T. 1996, A&A, 312, 365
Blandford, R. D., & Payne, D. G. 1982, MNRAS, 199, 883
Boselli, A., Cortese, L., Boquien, M., et al. 2014, A&A, 564, A67
Cappi, M. 2006, Astronomische Nachrichten, 327, 1012
Cardelli, J. A., Savage, B. D., Bruhweiler, F. C., et al. 1991, ApJ, 377, L57
Carniani, S., Marconi, A., Maiolino, R., et al. 2015, A&A, 580, A102
Castro, A., Miyaji, T., Shirahata, M., et al. 2014, PASJ, 66, 110
Cicone, C., Maiolino, R., Sturm, E., et al. 2014, A&A, 562, A21
Condon, J. J., Cotton, W. D., Greisen, E. W., et al. 1998, AJ, 115, 1693
Cutri, R. M., Skrutskie, M. F., van Dyk, S., et al. 2003, VizieR Online Data Catalog, 2246
Dasyra, K. M., Ho, L. C., Netzer, H., et al. 2011, ApJ, 740, 94
de Vaucouleurs, G., de Vaucouleurs, A., Corwin, Jr., H. G., et al. 1991, Third Reference Catalogue of Bright Galaxies. Volume I: Explanations and references. Volume II: Data for galaxies between 0^h and 12^h. Volume III: Data for galaxies between 12^h and 24^h.
Di Matteo, T., Springel, V., & Hernquist, L. 2005, Nature, 433, 604
Dopita, M. A., & Sutherland, R. S. 1995, ApJ, 455, 468
—. 1996, ApJS, 102, 161
ESA, ed. 1997, ESA Special Publication, Vol. 1200, The HIPPARCOS and TYCHO catalogues. Astrometric and photometric star catalogues derived from the ESA HIPPARCOS Space Astrometry Mission
Fabian, A. C. 2012, ARA&A, 50, 455
Feruglio, C., Fiore, F., Carniani, S., et al. 2015, A&A, 583, A99
Fu, H., & Stockton, A. 2007, ApJ, 666, 794
Fullmer, L., & Londsdale, C. J. 1989, Cataloged galaxies and quasars observed in the IRAS survey
Gallimore, J. F., Axon, D. J., O'Dea, C. P., Baum, S. A., & Pedlar, A. 2006, AJ, 132, 546
García-Burillo, S., Combes, F., Usero, A., et al. 2014, A&A, 567, A125
Gibson, R. R., Jiang, L., Brandt, W. N., et al. 2009, ApJ, 692, 758
Gofford, J., Reeves, J. N., Tombesi, F., et al. 2013, MNRAS, 430, 60
Gregory, P. C., Vavasour, J. D., Scott, W. K., & Condon, J. J. 1994, ApJS, 90, 173
Groves, B. A., Dopita, M. A., & Sutherland, R. S. 2004, ApJS, 153, 75
Hardcastle, M. J., Worrall, D. M., Kraft, R. P., et al. 2003, ApJ, 593, 169
Hashimoto, T., Nagao, T., Yanagisawa, K., Matsuoka, K., & Araki, N. 2011, PASJ, 63, L7
Heckman, T. M., Armus, L., & Miley, G. K. 1990, ApJS, 74, 833
Ho, I.-T., Kewley, L. J., Dopita, M. A., et al. 2014, MNRAS, 444, 3894
Ho, I.-T., Medling, A. M., Bland-Hawthorn, J., et al. 2016, MNRAS, 457, 1257
Ho, L. C., Filippenko, A. V., & Sargent, W. L. W. 1997a, ApJS, 112, 315
—. 1997b, ApJ, 487, 568
Imanishi, M., & Dudley, C. C. 2000, ApJ, 545, 701
Imanishi, M., & Wada, K. 2004, ApJ, 617, 214
Jackson, N., & Beswick, R. J. 2007, MNRAS, 376, 719
Kellermann, K. I., Sramek, R., Schmidt, M., Shaffer, D. B., & Green, R. 1989, AJ, 98, 1195
King, A. R. 2010, MNRAS, 402, 1516
Knop, R. A., Armus, L., Larkin, J. E., et al. 1996, AJ, 112, 81
Komossa, S., & Schulz, H. 1997, A&A, 323, 31
Konigl, A., & Kartje, J. F. 1994, ApJ, 434, 446
Koo, B.-C., & Lee, Y.-H. 2015, Publication of Korean Astronomical Society, 30, 145
Koo, B.-C., Lee, Y.-H., Moon, D.-S., Yoon, S.-C., & Raymond, J. C. 2013, Science, 342, 1346
Kormendy, J., & Ho, L. C. 2013, ARA&A, 51, 511
Kormendy, J., & Richstone, D. 1995, ARA&A, 33, 581
Krajnović, D., Sharp, R., & Thatte, N. 2007, MNRAS, 374, 385
Krolik, J. H., & Kriss, G. A. 2001, ApJ, 561, 684
Larkin, J. E., Armus, L., Knop, R. A., Soifer, B. T., & Matthews, K. 1998, ApJS, 114, 59
Laurent-Muehleisen, S. A., Kollgaard, R. I., Ryan, P. J., et al. 1997, A&AS, 122, 235
Magorrian, J., Tremaine, S., Richstone, D., et al. 1998, AJ, 115, 2285
Maiolino, R., Gallerani, S., Neri, R., et al. 2012, MNRAS, 425, L66
Marconi, A., & Hunt, L. K. 2003, ApJ, 589, L21
McAlary, C. W., McLaren, R. A., McGonegal, R. J., & Maza, J. 1983, ApJS, 52, 341
Miller, P., Rawlings, S., & Saunders, R. 1993, MNRAS, 263, 425

Mouri, H., Kawara, K., & Taniguchi, Y. 2000, ApJ, 528, 186
Murray, N., Chiang, J., Grossman, S. A., & Voit, G. M. 1995, ApJ, 451, 498
Nagao, T., Murayama, T., Shioya, Y., & Taniguchi, Y. 2003, AJ, 125, 1729
Nagao, T., Murayama, T., & Taniguchi, Y. 2001, PASJ, 53, 629
Nagao, T., Taniguchi, Y., & Murayama, T. 2000, AJ, 119, 2605
Nagar, N. M., Falcke, H., & Wilson, A. S. 2005, A&A, 435, 521
Nagar, N. M., Wilson, A. S., & Falcke, H. 2001, ApJ, 559, L87
Nomura, M., Ohsuga, K., Takahashi, H. R., Wada, K., & Yoshida, T. 2016, PASJ, 68, 16
Oi, N., Imanishi, M., & Imase, K. 2010, PASJ, 62, 1509
Oliva, E., Marconi, A., Maiolino, R., et al. 2001, A&A, 369, L5
Pereira-Santaella, M., Diamond-Stanic, A. M., Alonso-Herrero, A., & Rieke, G. H. 2010, ApJ, 725, 2270
Petric, A. O., Armus, L., Howell, J., et al. 2011, ApJ, 730, 28
Petrosian, A., McLean, B., Allen, R. J., & MacKenty, J. W. 2007, ApJS, 170, 33
Proga, D., Ostriker, J. P., & Kurosawa, R. 2008, ApJ, 676, 101
Ramos Almeida, C., Pérez García, A. M., & Acosta-Pulido, J. A. 2009, ApJ, 694, 1379
Ramos Almeida, C., Pérez García, A. M., Acosta-Pulido, J. A., et al. 2006, ApJ, 645, 148
Rees, M. J. 1984, ARA&A, 22, 471
Rich, J. A., Dopita, M. A., Kewley, L. J., & Rupke, D. S. N. 2010, ApJ, 721, 505
Riffel, R., Rodríguez-Ardila, A., & Pastoriza, M. G. 2006, A&A, 457, 61
Riffel, R. A., & Storchi-Bergmann, T. 2011, MNRAS, 417, 2752
Riffel, R. A., Storchi-Bergmann, T., & Nagar, N. M. 2010, MNRAS, 404, 166
Riffel, R. A., Storchi-Bergmann, T., & Riffel, R. 2015, MNRAS, 451, 3587
Riffel, R. A., Storchi-Bergmann, T., & Winge, C. 2013, MNRAS, 430, 2249
Riffel, R. A., Vale, T. B., Storchi-Bergmann, T., & McGregor, P. J. 2014, MNRAS, 442, 656
Risaliti, G., Maiolino, R., & Salvati, M. 1999, ApJ, 522, 157
Rodríguez-Ardila, A., & Viegas, S. M. 2003, MNRAS, 340, L33
Rupke, D. S. N., & Veilleux, S. 2011, ApJ, 729, L27
Sanders, D. B., & Mirabel, I. F. 1996, ARA&A, 34, 749
Schönell, A. J., Riffel, R. A., Storchi-Bergmann, T., & Winge, C. 2014, MNRAS, 445, 414
Schweizer, F., & Seitzer, P. 2007, AJ, 133, 2132
Silk, J., & Rees, M. J. 1998, A&A, 331, L1
Singh, V., Ishwara-Chandra, C. H., Wadadekar, Y., Beelen, A., & Kharb, P. 2015, MNRAS, 446, 599
Skrutskie, M. F., Cutri, R. M., Stiening, R., et al. 2006, AJ, 131, 1163
Sramek, R. 1975, AJ, 80, 771
Storchi-Bergmann, T., McGregor, P. J., Riffel, R. A., et al. 2009, MNRAS, 394, 1148
Taylor, G. B., Gugliucci, N. E., Fabian, A. C., et al. 2006, MNRAS, 368, 1500
Tody, D. 1986, in Society of Photo-Optical Instrumentation Engineers (SPIE) Conference Series, Vol. 627, Instrumentation in astronomy VI, ed. D. L. Crawford, 733
Tody, D. 1993, in Astronomical Society of the Pacific Conference Series, Vol. 52, Astronomical Data Analysis Software and Systems II, ed. R. J. Hanisch, R. J. V. Brissenden, & J. Barnes, 173
Tombesi, F., Cappi, M., Reeves, J. N., et al. 2010, A&A, 521, A57
Ulvestad, J. S., & Wilson, A. S. 1984, ApJ, 285, 439
Ulvestad, J. S., Wrobel, J. M., Roy, A. L., et al. 1999, ApJ, 517, L81
Véron-Cetty, M.-P., & Véron, P. 2010, A&A, 518, A10
Wagner, A. Y., Bicknell, G. V., & Umemura, M. 2012, ApJ, 757, 136
Wagner, A. Y., Umemura, M., & Bicknell, G. V. 2013, ApJ, 763, L18
Watabe, Y., Kawakatu, N., & Imanishi, M. 2008, ApJ, 677, 895
Weaver, K. A., Meléndez, M., Mushotzky, R. F., et al. 2010, ApJ, 716, 1151
Weymann, R. J., Morris, S. L., Foltz, C. B., & Hewett, P. C. 1991, ApJ, 373, 23
Whittle, M. 1992, ApJS, 79, 49
Wilson, A. S., & Raymond, J. C. 1999, ApJ, 513, L115
Wilson, A. S., & Willis, A. G. 1980, ApJ, 240, 429
Wu, Y.-Z., Zhao, Y.-H., & Meng, X.-M. 2011, ApJS, 195, 17
Yanagisawa, K., Shimizu, Y., Okita, K., et al. 2006, in Society of Photo-Optical Instrumentation Engineers (SPIE) Conference Series, Vol. 6269, Society of Photo-Optical Instrumentation Engineers (SPIE) Conference Series, 3
Yanagisawa, K., Okita, K., Shimizu, Y., et al. 2008, in Society of Photo-Optical Instrumentation Engineers (SPIE) Conference Series, Vol. 7014, Society of Photo-Optical Instrumentation Engineers (SPIE) Conference Series, 37
Zwicky, F., & Kowal, C. T. 1968, "Catalogue of Galaxies and of Clusters of Galaxies", Volume VI